Soft Matter

PAPER

View Article Online
View Journal | View Issue

Cite this: *Soft Matter*, 2023, **19**, 6569

Lipid doping of the sponge (L_3) mesophase†

Christopher Brasnett, ‡[a] Adam M. Squires, [c] Andrew J. Smith [d] and Annela M. Seddon *[ab]

Received 3rd May 2023,
Accepted 14th August 2023

DOI: 10.1039/d3sm00578j

rsc.li/soft-matter-journal

The polymorphism of lipid aggregates has long attracted detailed study due to the myriad factors that determine the final mesophase observed. This study is driven by the need to understand mesophase behaviour for a number of applications, such as drug delivery and membrane protein crystallography. In the case of the latter, the role of the so-called 'sponge' (L_3) mesophase has been often noted, but not extensively studied by itself. The L_3 mesophase can be formed in monoolein/water systems on the addition of butanediol to water, which partitions the headgroup region of the membrane, and decreases its elastic moduli. Like cubic mesophases, it is bicontinuous, but unlike them, has no long-range translational symmetry. In our present study, we show that the formation of the L_3 phase can delicately depend on the addition of dopant lipids to the mesophase. While electrostatically neutral molecules similar in shape to monoolein (DOPE, cholesterol) have little effect on the general mesophase behaviour, others (DOPC, DDM) significantly reduce the composition at which it can form. Additionally, we show that by combining cholesterol with the anionic lipid DOPG, it is possible to form the largest stable L_3 mesophases observed to date, with characteristic lengths over 220 Å.

1 Introduction

One of the principle motivations for the study of self-assembled lipid systems is their astonishing range of potential applications, ranging from templating and drug delivery, to membrane protein crystallisation.[1–6] Of these, membrane protein crystallisation using the so-called *in meso* or lipid cubic phase (LCP) method has long been cited as a principal source of motivation for studies of lipid polymorphism.[7–15]

Self-assembled lipid aggregates can exhibit a number of different symmetries shown in Fig. 1(a)–(d), from the planar 1 dimensional lamellar bilayer stacks (L_α), 2 dimensional arrays of hexagonally arranged cylinders, or 3 dimensional cubic phases. In triply periodic bicontinuous cubic phases, the lipid bilayer spans a triply periodic minimal surface, a surface defined by having zero mean curvature at all points, and separates the system bicontinuously into two water channels.[16] Three bicontinuous cubic phases are known, the Primitive (Q_{II}^P), Diamond (Q_{II}^D), and Gyroid (Q_{II}^G). In addition to these extensively-studied mesophases, the sponge (L_3) mesophase is occasionally observed upon the addition of other molecules to the monoolein/water system. Mesophases have characteristic small angle X-ray scattering (SAXS) patterns according to their topology and size.[17] In the case of the L_3 mesophase, the position of the centre of the characteristic broad peak measured using SAXS is related to the cell dimensions of the system.[18–21]

The sponge phase is known to be closely related to the cubic phase, similarly consisting of a lipid bilayer separating bicontinuous water channels, but without long-range translational symmetry.[22–25] Cherezov *et al.*[26] showed that a number of additives to the monoolein (MO)/water system can form the sponge phase in lipid systems, a common feature among one class in particular being that they are small amphiphiles with a number of both hydrogen bond acceptors and donors.[26] This enables them to interact with both the water channels of the Q_{II}^D mesophase as well as the hydrophobic region of the membrane, later confirmed in ^{1}H NMR studies by Evenbratt *et al.*[27] The net effect of these interactions is the swelling of the Q_{II}^D mesophase as the interface is partitioned by the additives and flattened. Beyond a certain concentration when the bending modulus of the membrane is lowered, the Q_{II}^D mesophase becomes disordered and the system becomes a L_3 mesophase. Upon further increase of the sponge-forming additive, a flat L_α mesophase will emerge.

[a] *School of Physics, University of Bristol, Tyndall Avenue, Bristol, BS8 1FD, UK. E-mail: annela.seddon@bristol.ac.uk*
[b] *Bristol Centre for Functional Nanomaterials, School of Physics, University of Bristol, Tyndall Avenue, Bristol, BS8 1FD, UK*
[c] *Department of Chemistry, University of Bath, Bath, BA2 7AY, UK*
[d] *Diamond House, Diamond Light Source Ltd, Harwell Science and Innovation Campus, Fermi Ave., Didcot, OX11 0DE, UK*

† Electronic supplementary information (ESI) available: Supplementary information contains all scattering patterns for the data discussed, and details on structural parameter calculations. See DOI: https://doi.org/10.1039/d3sm00578j

‡ Present Address: Groningen Biomolecular Sciences and Biotechnology Institute, University of Groningen, Groningen, The Netherlands.

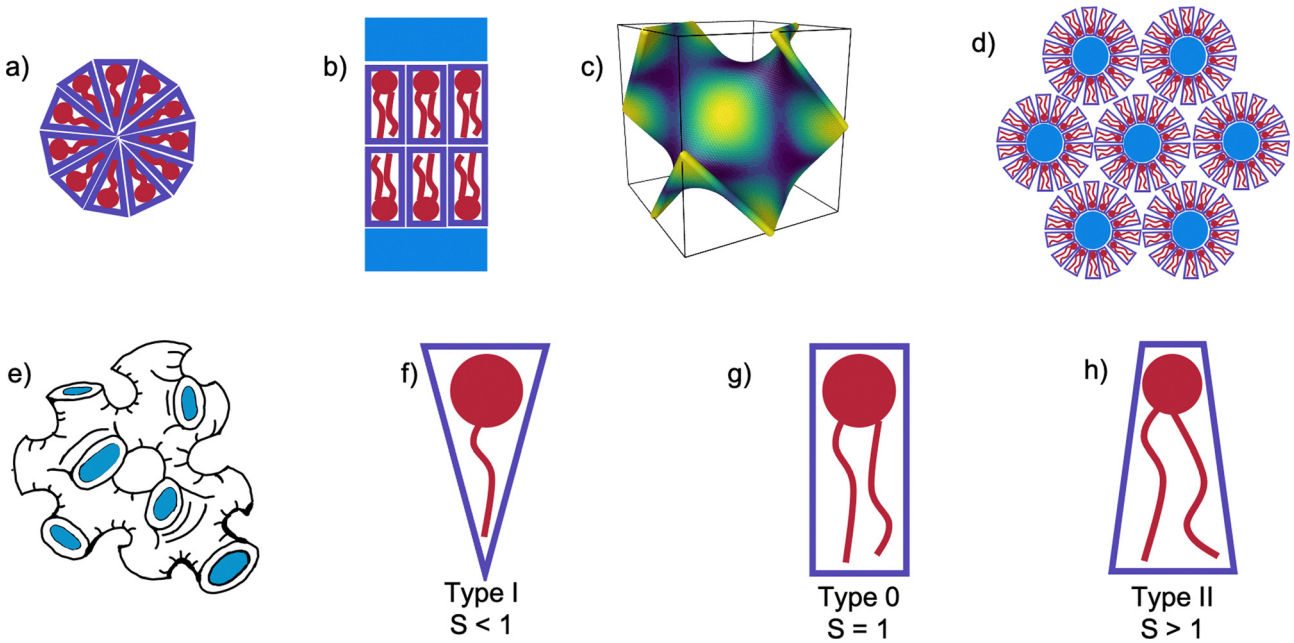

Fig. 1 Illustrations of possible self-assembled mesophases and packing types of lipids and surfactants. (a) A micelle, (b) a flat bilayered L_α mesophase surrounded by water channels, (c) a Q_{II}^D minimal surface (coloured according to Gaussian curvature: light patches flat and dark more curved), (d) a Hexagonal (H_{II}) mesophase, with blue water channels extending in and out of the page, (e) a sponge (L_3) mesophase with water channels highlighted in blue, (f) a type I molecule, with $S < 1$, (g) a type 0 molecule with $S = 1$, (h) a type II molecule with $S > 1$.

One of the greatest successes of the LCP technique to date has been the solution of the structure of the human β_2 adrenergic G-protein-coupled receptor.[28,29] The high-throughput screening techniques used in these studies for finding successful crystallisation conditions noted that including a significant proportion of cholesterol in the mesophase was essential for crystal growth. In the case of crystallisation of the entire protein complex, crystals were harvested from a 'sponge-like mesophase'. While the mesophase was not explicitly characterised, the addition of PEG400 is known to induce this transition, so it is likely that this was the case.[30–32] Similarly, crystallisation of human microsomal prostaglandin E2 synthase 1 by Li *et al.*[33] found that doping the monoolein membrane at a level of 5% mol with DOPC, a zwitterionic phospholipid, was essential to guarantee successful crystallisation.[33]

To add to the significance of the sponge phase, other membrane proteins had previously been crystallised from the sponge phase directly, but the solution of the human β_2 adrenergic G-protein-coupled receptor demonstrates the significance of the method.[34–36] Understanding the exact mechanisms of LCP remains an area of extensive study, with Zabara *et al.*[37] demonstrating that the sponge phase can play an important intermediary role in the crystallogenesis of membrane protein crystals.[37]

The mesophase behaviour of monoolein has been extensively studied on its own, forming a Q_{II}^D mesophase in excess water at room temperature, and undergoing a transition to the H_{II} mesophase when heated.[38,39] In addition to studying the mesophase behaviour of monoolein alone, many studies have additionally investigated the effect of lipid type doping on the structure of the self-assembled behaviour of lipid systems, and for an excellent review we refer the interested reader to the work of van't Hag *et al.*[14] Lipid type refers to the categorisation of lipids and surfactants according to their packing parameter, S[40]:

$$S = \frac{v}{al} \quad (1)$$

where v is the volume of the hydrocarbon tails, a the interfacial surface area, and l the maximum effective tail length. Molecules can then be catagorised depending on their value of S, as we show in Fig. 1(f)–(h), which is a key determinant in the self-assembled mesophase that results from aggregates of molecules of that type. For $S < 1$, the interfacial area is relatively large, and a positively curved membrane where the membrane curves away from its hydrophobic region results. Conversely, molecules with $S > 1$ will have negatively curved interfaces. For $S = 1$, cylindrical-like molecules will result in planar bilayered systems. When added to cubic phases, Cherezov *et al.*[41] showed that generally, the cubic phase can hold up to around 20% mol doping of an additional lipid before reverting to the preferred mesophase of the dopant.[41]

One of the main barriers to the success of the LCP method is the small water channels of the cubic phase.[42] Attempts to overcome this have often used lipids with charged headgroups in order to promote intra-bilayer electrostatic repulsion as to increase the size of the lattice parameter, and flatten the cubic phase observed to a Q_{II}^P.[12] In contrast, our recent work has demonstrated that the addition of common salts at low concentrations will screen intra-bilayer charge repulsion, and so revert the mesophase of the lipid system back to the Q_{II}^D.[43]

However, it is likely that the crystallisation process could still further disturb the mesophase behaviour through the addition of precipitating salts. Although this could suggest that experiments to understand membrane dynamics are in and of themselves naive, the incorporation of membrane protein into a membrane prior to crystallisation would remain significant, and so seeking to understand the compositional factors affecting mesophase behaviour remains a worthwhile pursuit.

Noting that the adaptability of the sponge phase is a little-understood area, in the present work we investigate lipid type doping of the sponge phase, using several common lipid and detergent additives. The possibility of doping the sponge phase has been noted in direct sponge phase crystallisation trials, where the use of 1% w/w cholesterol was necessary for successful crystallisation of a bacterial photosynthetic core complex.[35] While it would be ideal to screen every possible crystallisation condition for the mesophase behaviour, we can seek to understand a broader set of design rules by understanding the conditions under which the L_3 mesophase forms.

Furthermore, the variation of the characteristic length of the L_3 mesophase is little understood in comparison to the wealth of similar studies on the topic of bicontinuous cubic lattice parameters.[12,41,44–46] As one of the significant barriers to the LCP crystallisation of membrane proteins with large hydrophilic domains is the small water channels of lipid cubic phases, the dependence of the characteristic lengths – and therefore size of water channels – of L_3 mesophases on dopants is a significant challenge to the field. Angelov *et al.*[47] describe the formation of lipid L_3 mesophases with characteristic lengths between 35–40 Å, which are of a similar length to those more recently studied by Bhattacharya *et al.*[20,47] With broad peaks centered at around 0.05 $Å^{-1}$, representing a characteristic length of around 125 Å, a recent study by Talaikis *et al.*[48] has found slightly larger lipid L_3 mesophases, but a systematic study of the variation of this length remains lacking from the literature.[48]

To rectify the above omissions from our current understanding of the L_3 mesophase, in this work we investigate the effect on the Q_{II}^D/L_3 transition on doping monoolein with several common additive molecules of different packing parameters and biological applications: cholesterol, dioleoylphosphoethanolamine (DOPE), dioleoylphosphocholine (DOPC), and n-Dodecyl β-D-maltoside (DDM). In addition, we use a combination of the anionic dioleoylphosphoglycerol (DOPG) and cholesterol together, after Tyler *et al.*,[12] to maximise the lattice parameters obtained.[12]

2 Materials and methods

Monoolein (MO) was received as gift from Danisco and used without further preparation. Cholesterol and DDM were purchased from Sigma Aldrich in powdered form. 1,4-Butanediol was purchased from Sigma Aldrich. DOPC, DOPE, DOPG were purchased from Avanti Polar Lipids in powdered form. Lipids (aside from DDM) were prepared in dichloromethane at concentrations of 0.1 M, and mixed at the required doped molarities. DDM was prepared in ethanol at a concentration of 0.05 M. Monoolein was prepared at both 0.1 M and 0.05 M concentrations, and 2.5%, 5%, 7.5%, and 10% mol doped monoolein solutions were then prepared volumetrically. 70 μL of doped lipid mixtures in solvent were transferred to 1.5 mm X-ray capillaries (Capillary Tube Supplies UK Ltd), and left to evaporate for 3 days. The remaining solvent was removed under vacuum, leaving a film of dried mixed lipid on the capillary walls, before the addition of 50 μL of solvent, so that the samples were hydrated under excess solvent conditions. The capillaries were then sealed, and put through 3 freeze–thaw cycles to ensure the sample was at equilibrium before measurement. Preparation of X-ray capillaries under vacuum is known to have significant effects on mesophase behaviour, so this last step ensured that no out of equilibrium effects were measured.[44]

We chose to measure the self-assembled mesophase at 9 volume/volume proportions of butanediol/water solvent content: 0%, 20%, 32.5%, 35%, 37.5%, 40%, 42.5%, 45%, 47.5%. For monoolein alone, the Q_{II}^D/L_3 transition is known to occur at 30% v/v butanediol, and the L_3/L_α transition at 50% v/v.[26] This selection of solvents therefore allows us to understand the mesophase behaviour in (i) water alone, (ii) a point significantly below the expected transition, in case any significant anomalous behaviour is observed, and (iii) a granular range of solvents in a region where the sponge phase is known to exist, in order to observe the lowering of the second transition.

SAXS measurements were performed on a SAXSLAB Ganesha 300XL instrument with a q range of 0.015–0.65 $Å^{-1}$ for 600 s per sample. All scattering patterns measured are plotted in the ESI.† Mesophases and their characteristic lengths were determined from their characteristic Bragg peak spacings (in the case of mesophases with translational symmetries) or the positions of their broad peaks (as in the case of the L_3 mesophase and micellar systems) measured with SAXS, as detailed in S1 of the ESI.† Bragg peaks were found using Python scripts written in-house and available at **https://github.com/csbrasnett/lipidsaxs**.

3 Results and discussion

3.1 Monoolein sponge phases

In Fig. 2, we validate the well-known result of Cherezov *et al.*[26] of the mesophase behaviour of the MO/water/butanediol system.[26] On the initial addition of butanediol to a proportion of 20% v/v of the solvent, the size of the Q_{II}^D mesophase swells from 97 Å to 123 Å in water. In our focused range between 32.5% and 47.5% butanediol, we observe a sponge phase with a characteristic length increasing linearly from 100 Å to 154 Å. As a confirmation of the literature on these lyotropic conditions, we have demonstrated the validity of our capillary evaporation method for sample preparation.

To form the L_3 meosphase, Cherezov *et al.*[26] use a set ratio of lipid : solvent of 60 : 40% weight/weight, the excess water point

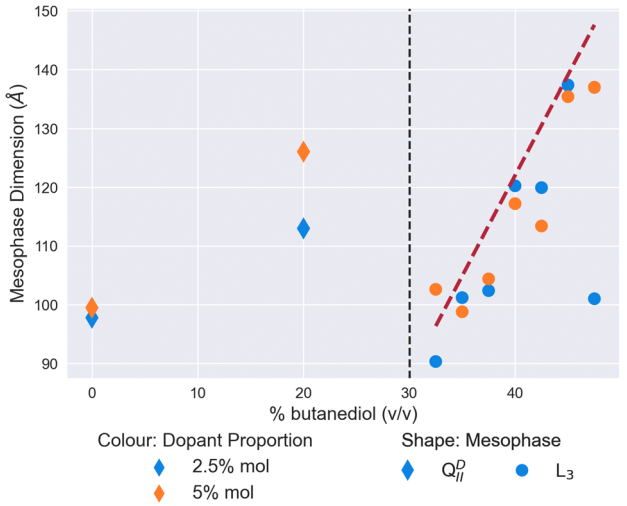

Fig. 2 The mesophase and size behaviour of a system of monoolein and a solvent of butanediol and water, with increasing proportions of butanediol in the solvent. The shape of the scatter point indicates the mesophase, a Diamond for the Q_{II}^{D} mesophase and a circle for the L_3 mesophase. The red dashed line is a linear regression to the L_3 mesophase data as a guide.

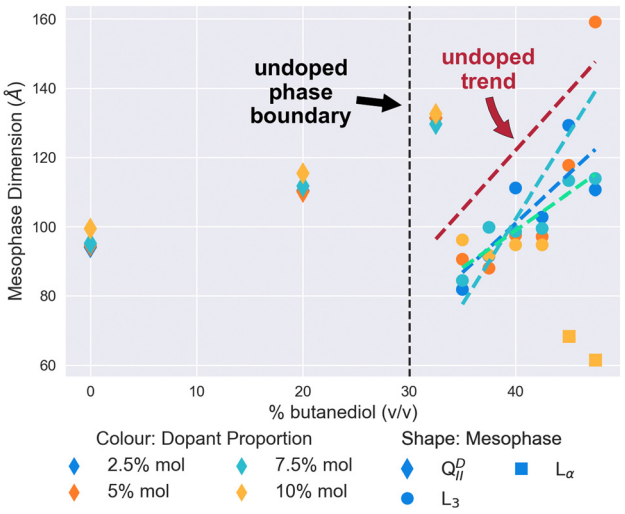

Fig. 3 The mesophase and size behaviour of cholesterol-doped monoolein systems changing as butanediol is introduced into the system. Molar proportion of dopant is indicated by colour: 2.5% (Blue), 5% (Turquoise), 7.5% (Green), and 10% (Yellow). The shape of the scatter point indicates the mesophase: Q_{II}^{D} (Diamond), L_3 (Circle), L_α (Square). Dashed lines have been fitted using linear regression as a guide for the trend of the characteristic length of the L_3 mesophases, and coloured accordingly. In addition, the Red dashed line is the linear regression to the pure monoolein L_3 mesophases seen in Fig. 2 as a reference. The vertical black dashed line at 30% v/v indicates the position of the Q_{II}^{D}/L_3 transition in a pure monoolein lipid system.

of monoolein in water.[26,39] To validate our excess solvent method, we measured the characteristic lengths of sponge phases at 3 excess weight ratios, and observed no significant change (±10 Å, see Fig. S1 in ESI†). This demonstrates that the results throughout this work will be valid for any excess hydration conditions.

3.2 Effect of single dopants on the formation of the L_3 mesophase

3.2.1 A common co-crystallisation dopant: cholesterol. Fig. 3 shows how the doping of monoolein with cholesterol affects the phase behaviour and size of the self-assembled mesophase as the proportion of butanediol in the solvent is increased. For a simple ternary MO/H_2O/butanediol system, the Q_{II}^{D}/L_3 phase change is expected at 30% v/v butanediol. In cholesterol-doped systems, the Q_{II}^{D} phase swells from a lattice parameter of around 100 Å to between 110 Å and 120 Å on an initial increase of butanediol in the solvent to 20% v/v. Upon further increase in the butanediol content of the solvent however, the cholesterol-doped systems demonstrate a shift in the Q_{II}^{D}/L_3 mesophase boundary from 30% v/v to above 32.5% v/v. Cholesterol is known to condense and stiffen membranes, so it is likely that these factors promote the stability of the Q_{II}^{D} mesophase beyond the undoped meosphase boundary.[49–52]

Subsequent increases in the butanediol content of the solvent to 35% v/v and above results in the cholesterol-doped systems undergoing a mesophase transition to the L_3 mesophase. At all proportions of dopant, as Fig. 3 demonstrates, this transition to cholesterol-doped L_3 mesophase results in a reduction of the L_3 characteristic lengths in comparison to undoped L_3 mesophases. Again, this could similarly be explained by the stiffening effect that cholesterol has on the membrane. A recent study by Chakraborty *et al.*[49] showed that as the cholesterol content of vesicles is increased, the relative bending rigidity does so correspondingly.[49] In the context of this work, an increase in bending rigidity would explain why the L_3 characteristic length is mostly reduced in comparison to the L_3 phases we see in undoped systems. As the Gaussian bilayer bending modulus is dependent on spontaneous curvature, an increase in bending modulus is therefore likely to increase the Gaussian curvature of the system, therefore bring bilayers closer together, and reducing the characteristic length of the L_3 mesophase observed.[8]

Perhaps the most notable feature of the cholesterol-doped systems in the solvent range examined is the emergence of the L_α mesophase at high concentrations of cholesterol. As shown in Fig. 3, at a level of 10% mol cholesterol doping, the system undergoes a second phase transition from the L_3 to the L_α at a butanediol solvent concentration of 45% v/v. Cherezov *et al.*[41] found that above a 20% mol doping, cholesterol-doped monoolein will both form a flatter Q_{II}^{P} mesophase and precipitate out of the membrane into crystals of cholesterol monohydrate.[41] Although in comparison we only observed this phenomenon at 10% mol, it is likely that thermal fluctuations will affect the stability of the L_3 mesophase significantly, so it is unsurprising that we similarly observe a transition to a flatter mesophase at reduced solvent conditions.

3.2.2 Two common phospholipids: DOPE & DOPC. As common biological membrane phospholipids, it could be expected that DOPE and DOPC act as essential cocrystallised lipids in LCP trials for a wide number of membrane proteins. In order to understand the effect that they have on L_3 mesophases,

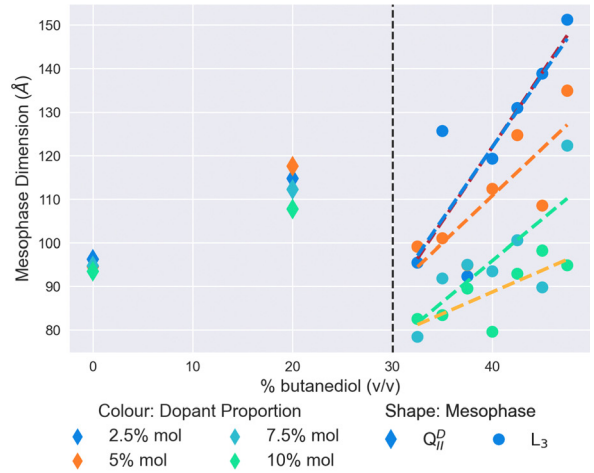

(a) DOPE-doped mesophase behaviour

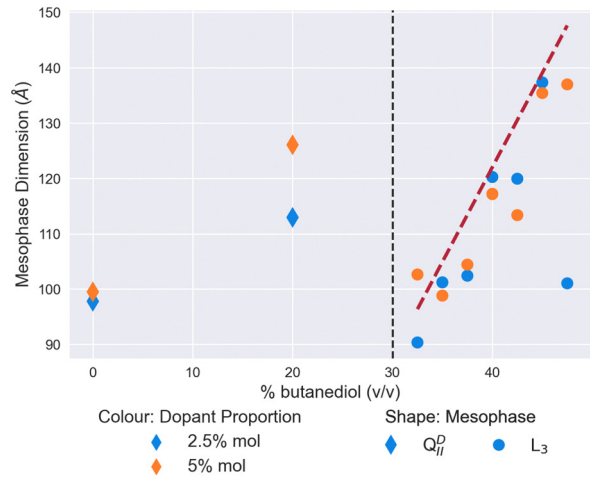

(b) MO doped with DOPC at 2.5%, 5% mol

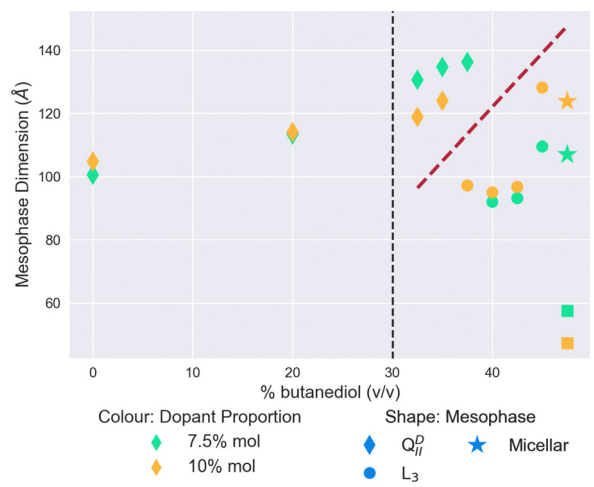

(c) MO doped with DOPC at 7.5%, 10% mol

Fig. 4 The mesophase and size behaviour of MO with (a) DOPE, (b) low doped proportions (2.5%, 5% mol) of DOPC and (c) high doped proportions of DOPC (7.5%, 10% mol) with varying proportions of butanediol in the solvent. The molar proportions are indicated by the colour of the scatter points, and the mesophase by their shapes. The dashed vertical black lines indicate the location of the Q_{II}^D/L3 transition in a system of MO alone.

we repeated the cholesterol doping experiments using both these phospholipids, the results of which are shown in Fig. 4.

Of all the dopants studied in this work, the mesophase sequence behaviour of DOPE-doped systems, shown in Fig. 4a is the least modified in comparison to the undoped one shown in Fig. 2. There is no observable shift in the position of the Q_{II}^D/L_3 mesophase boundary, with data below these points exhibiting a clear Q_{II}^D mesophase, and a L_3 mesophase above this point. Moreover, unlike the cholesterol-doped systems, we observed no further transition to the L_α mesophase at any either butanediol solvent proportion or dopant concentration.

Where DOPE-doped systems do differ, however, is in the clear trend that these systems have for the reduction in the L_3 mesophase characteristic length in correspondence to the increase in the concentration of dopant molecules in the membrane. Indeed, at 47.5% v/v butanediol, there is a decrease from 151 Å to 94 Å of the L_3 characteristic length on increasing the dopant proportion from 2.5% to 10% mol. In comparison in water, a DOPE-doped MO system reduces the lattice parameter of the Q_{II}^D mesophase before inducing a mesophase transition at 20% mol.[41] While the authors note that in cubic phases, lattice size is a non-trivial function of spontaneous curvature, the extent of the reduction observed here suggests that it has a significant influence. A reduction in the characteristic length of the L_3 mesophase is suggestive of a more tightly arranged structure (*i.e.* highly curved) between successive 'necks' of the membrane, likely driven by the greater wedge shape of the type II DOPE dopant.

In contrast to the relatively simple and unmodified phase sequence that are observed by doping with DOPE, the mesophase behaviour for monoolein doped with the type 0 lipid DOPC is significantly more complex. We show the results in Fig. 4b and c, split between lower levels of doping (Fig. 4b) and higher levels (Fig. 4c). As one expects in both cases, the initial introduction of butanediol into the solvent merely swells the size of the Q_{II}^D mesophase observed rather than brings about a mesophase transition.

At lower proportions of DOPC in the membrane (Fig. 4b), the Q_{II}^D/L_3 transition does not appear to shift with respect to the point for monoolein L_3 phases alone. Interestingly, the L_3 characteristic lengths subsequent to the transition are of a comparable length to the undoped data. This similarity is notable in comparison to the slight reductions observed at these proportions seen in DOPE-doped systems, as it further demonstrates the effect the shape parameter has on the resultant L_3 mesophase. As a type 0 lipid, the increased system-mean head group area in DOPC-doped systems promotes less curved membranes, and therefore L_3 mesophases with increased characteristic lengths.

On increasing the proportion of DOPC in the membrane as shown in Fig. 4c, the Q_{II}^D/L_3 transition point is significantly increased to 37.5% v/v butanediol for 10% mol DOPC, and 40% v/v butanediol for 7.5% mol DOPC. Molecular dynamics and spectroscopy studies investigating the water/lipid interface have shown that phosphocholine headgroups allow for a looser packing of water at the interface, and that hydrogen bonds can

be formed between the phosphocholine carbonyl groups and water.[53–57] Evenbratt *et al.*[27] showed using ^{1}H NMR that diols form the L_3 phase by molecular partitioning at the polar/non-polar interface.[27] The introduction of high levels of DOPC therefore increases the hydration of the bilayer at the interface, at the expense of the presence of butanediol, and so the Q_{II}^D mesophase is sustained for higher proportions of butanediol in the solvent than is otherwise expected. This increased presence of water is corroborated by the larger lattice parameters for Q_{II}^D mesophases observed above 30% v/v butanediol, which implies a flatter (less curved) membrane and more hydrated interface.

Considering the increased hydration of the interface with the introduction of more DOPC, it is perhaps surprising that the L_3/L_α transition is not reduced correspondingly. We only observed a system of coexisting (normal) micelles and L_α mesophases for both dopant levels at 47.5% v/v butanediol. As Fig. 4c shows, for both the higher proportions of DOPC, we only observed a L_3/L_α transition at 47.5% v/v butanediol for both systems, where there is also coexistence with micelles. As a type 0 lipid, DOPC has a larger headgroup to begin with than monoolein, which could be expected to lower this transition accordingly. That the transition is only lowered slightly suggests that there is a delicate interplay in this transition between the role of headgroup size and the partitioning effect of butanediol. The coexisting micelles are likely a result of the shape mismatch between monoolein and DOPC in the membrane, which in the presence of butanediol, could self-assemble into micelles in order to maximise aggregate curvature outside of the primary membrane system.

3.2.3 A common protein detergent: DDM. The addition of DDM to monoolein in water at sufficient concentration is known to destabilise the Q_{II}^D mesophase induce a transition to the L_α phase.[58–60] A Q_{II}^G mesophase is observed at intermediate concentrations, as a result of molecular shape mismatch: the Q_{II}^G mesophase has the largest interfacial surface area of any of the cubic phases.[17]

We plot the results for lower- and higher- doped systems in Fig. 5a and b respectively. In contrast to DOPE, cholesterol, or DOPC, the addition of butanediol to the solvent in lower-doped systems does not appear to have any significant swelling effect on the Q_{II}^D lattice parameter, although the addition of 5% DDM in water increases the size of the Q_{II}^D seen to 145 Å, which is maintained at 20% v/v butanediol. Unlike in water, we did not observe a Q_{II}^G mesophase at any DDM proportion, with all dopant concentrations producing Q_{II}^D mesophases. Above 30% v/v butanediol, we observed a transition to the L_3 mesophase for both 2.5% mol and 5% mol doped systems. However as the proportion of butanediol is further increased, the mesophase behaviour of the lower-doped systems diverges. The 2.5% mol doped system continues in the L_3 phase, while for the 5% mol doped system, the L_3/L_α mesophase transition is significantly lowered to 35% v/v butanediol, where it coexists with normal micelles. In comparison, the 2.5% mol system only sees this transition at 47.5% v/v butanediol, the same solvent conditions for very highly-doped systems of DOPC (Fig. 4c).

On further increasing the proportion of DDM in the membrane more, the destabilising effect of DDM is immediately observed. While at 7.5% mol, the system in water remains in the Q_{II}^D mesophase, at 10% mol, the system has transformed into a coexisting L_α and micellar system. The 7.5% mol system also exhibits this at 20% v/v butanediol, and this is subsequently observed for both strongly-doped systems above 30% v/v. The subsequent increase in butanediol proportion in the solvent further demonstrates the incompatibility of DDM with MO-based mesophases, as the system continues to solely exhibit normal micelles and L_α mesophases.

3.3 Using electrostatics to form sponge phases

In addition to the 4 dopants described above, we also considered the possible effect of combining the anionic lipid DOPG with cholesterol on L_3 mesophases. Studies using DOPG as a

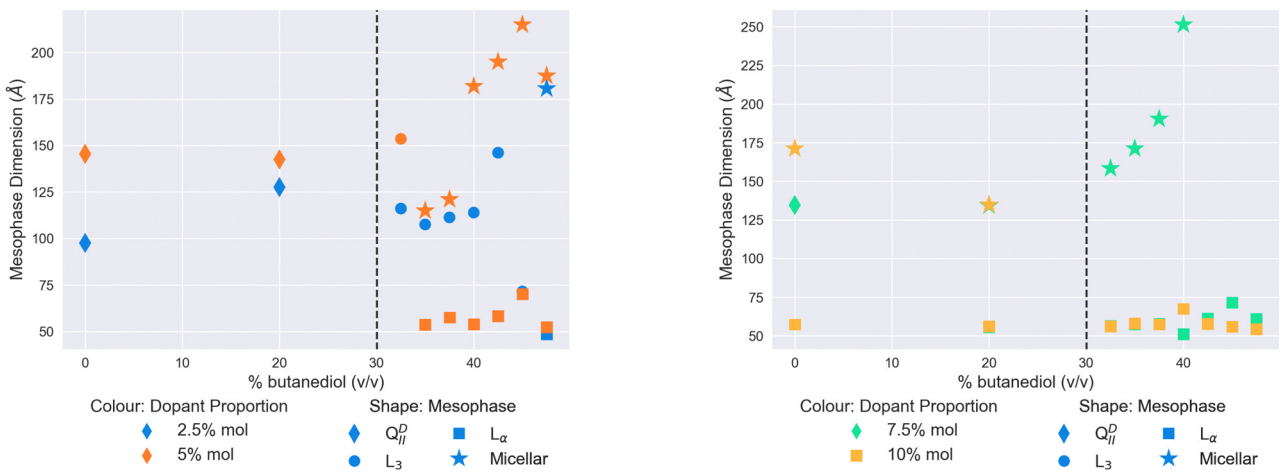

(a) MO doped with DDM at 2.5%, 5% mol

(b) MO doped with DDM at 7.5%, 10% mol

Fig. 5 The mesophase and size behaviour of MO doped with (a) low (2.5%, 5% mol) proportions of DDM, (b) high (7.5%, 10% mol) proportions of DDM with varying proportions of butanediol in the solvent. The dopant proportion is indicated by the colour of the scatter point, and the mesophase by its shape. The vertical dashed lines indicate the location of the Q_{II}^D/L_3 transition in a system of only MO.

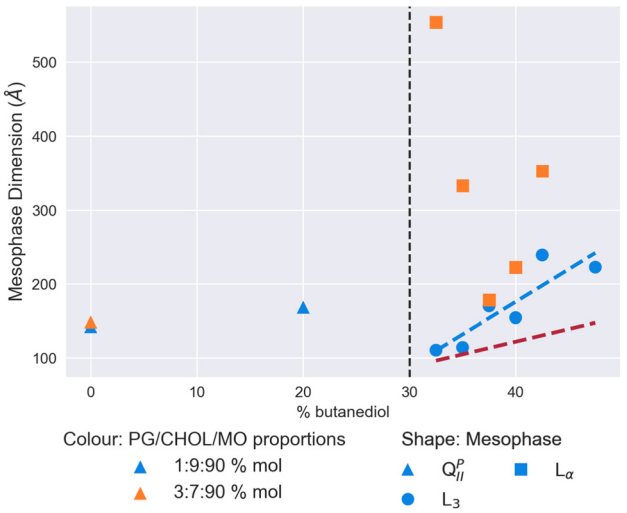

Fig. 6 Mesophase and size behaviour of monoolein doped with DOPG and cholesterol with a solvent of increasing butanediol content. The dashed red line shows the trend for the MO/water/butanediol system measured in Fig. 2, and the dashed blue line a linear regression to the L_3 mesophase data for the 1/9/90 DOPG/cholesterol/MO% mol system. The vertical dashed black lines indicate the location of the Q_{II}^{D}/L_3 transition for an undoped MO lipid system.

single dopant resulted in a variety of scattering patterns, shown in the ESI† as Fig. S22–S24. These scattering patterns show little discernible structure, and there is little clear evidence of such mesophase transition sequence as the Q_{II}^{D}–L_3–L_α observed with other single dopants. Insofar as there is evidence of mesoscale self-assembled structure, it is possible to identify Q_{II}^{P} mesophases upon addition of low quantities of butanediol, with Bragg peaks at ratios of $\sqrt{2}$:$\sqrt{4}$:$\sqrt{6}$, and L_α mesophases at several high proportions of butanediol addition. In between, however, there is little to no signal present – at least in the q-range it is possible to measure – and it is not possible to determine a definitive mesophase from the data available. If very large mesophases do exist outside of the measured range, it may be possible that recent synchrotron USAXS techniques could be used to determine their structure.[61] We therefore took inspiration from the ternary system of MO, DOPG, and cholesterol, previously used by Tyler *et al.*[12] to create some of the largest lipid cubic phases observed, showing that a mixture of 80/15/5 MO/cholesterol/PG heated to 45 °C adopts a Q_{II}^{P} phase with a lattice parameter of 415 Å. As these results suggest that the effect of even a small proportion of DOPG in the membrane is significant, we chose to use two high molar ratios of cholesterol to DOPG while keeping the proportion of MO the same in order to maximise chances of observing the L_3 mesophase in the solvent sequence.

We show both sets of results in Fig. 6. A L_3 mesophase was only observed in the system with 1% mol DOPG and 9% mol cholesterol. On changing this ratio to 3% mol and 7% mol respectively, we observed extremely large L_α mesophases, in one instance with a lattice parameter of over 500 Å, and consistently over 200 Å. Where we did observe the L_3 phase in the first system, it had a consistently larger characteristic length than we observe for MO alone in Fig. 2. Over the solvent range from 32.5% v/v butanediol to 47.5%, the characteristic length grows from 110 Å to 222 Å, with a peak of 239 Å observed at 42.5%. Therefore, the condensing effect of cholesterol previously observed in Fig. 3 can be used advantageously to stabilise electrostatically-doped systems to result in the largest L_3 mesophases observed to date.

4 Conclusions

We have demonstrated that the lipid L_3 sponge mesophase can successfully and stably be doped with additive lipids. A summary phase diagram of the four single dopants is shown in Fig. S2 (ESI†). In most cases, we have shown that the presence of additive lipids shrinks the characteristic length of the L_3 mesophase. This finding will have significance for designing LCP trials, as proteins with both large extracellular domains and essential co-crystallisation lipids will need to have the membrane environment carefully tailored to maximise the chances of successful crystallisation. However, we have also shown that use of electrostatic lipids such as DOPG can be used in conjunction with cholesterol to significantly increase the characteristic lengths of L_3 mesophases. Using these cholesterol-stabilised electrostatically-doped mesophases, we have observed sponge phases with characteristic lengths of around 240 Å, significantly larger than in MO alone. These results will should help inform the engineering design rules for future LCP crystallisation trials.

Regarding the Q_{II}^{D}/L_3 transition itself, here we have shown that the transition is sensitive to both the average headgroup area of the membrane and the bending modulus, indicating that the shape parameter S plays a critical role in regulating the transition. In the case of the headgroup area, we have shown that by increasing the interfacial area per molecule in the system increases the proportion of sponge-forming agent required in comparison to L_3 mesophases formed of MO alone. Similarly, using cholesterol - known to increase membrane moduli – slightly increases the proportion of sponge-forming agent required. DDM – which destabilises the monoolein Q_{II}^{D} mesophase by inducing a transition to the Q_{II}^{G} mesophase - drastically reduces the ability for L_3 mesophases to form. This is a particularly significant result, as it suggests that membrane proteins purified using DDM as a detergent could have a significant effect on the ability of those proteins to be incorporated into a monoolein host membrane, and subsequent crystallisation.

Techniques used to study the L_3 mesophase in recent years have mainly been limited to SAXS, such that the transition and relationships between the Q_{II}^{D} and the L_3 mesophases are studied statically. In future, methods to study the L_3 mesophase could take into account the dynamic nature of the phase transition, by investigating the structural rearrangement of lipid molecules in the process through techniques such as molecular dynamics.

In the context of LCP crystallisation, this study has shown that while many previous studies have been able to dramatically increase the lattice parameter of cubic phases using anionic doping, the effect of other crystallisation additives can prove to be otherwise counter productive. While it is impractical to investigate the combined effect of every possible crystallisation screen, we have shown here that in particular, the inclusion of cholesterol can stabilise electrostatically charged systems. These results should help inform future LCP trials where the need for large water channels is key to successful crystallisation conditions.

To further emphasise the increasing importance of an understanding of the L_3 mesophase, the advent of X-ray free electron lasers (XFELs) suggests that the direct use of the L_3 mesophase will become more important in future.[62–65] In this technique, the fluid properties of the L_3 mesophase are taken advantage of to flow small droplets of membrane protein embedded in a lipid L_3 mesophase-based crystals into a pulsed X-ray source. The understanding of the dynamics affecting the structure of the L_3 mesophase presented in this work is therefore instructive with the design of XFEL protein structure experiments.

Conflicts of interest

There are no conflicts to declare.

Acknowledgements

The Ganesha X-ray scattering apparatus used for this research was purchased under EPSRC Grant 'Atoms to Applications' Grant ref. EP/K035746/1. CB acknowledges studentship funding from EPSRC EP/N509619/1. We are grateful to Diamond Light Source for beam time awards (SM17767-1 and SM29558-1) to this project and to the staff, particularly Nick Terrill and Sam Burholt, on beamlines I22 and DL-SAXS for their support.

References

1 S. Akbar, J. M. Elliott, M. Rittman and A. M. Squires, *Adv. Mater.*, 2012, **25**, 1160–1164.
2 R. Mezzenga, J. M. Seddon, C. J. Drummond, B. J. Boyd, G. E. Schröder-Turk and L. Sagalowicz, *Adv. Mater.*, 2019, **31**, 1900818.
3 H. M. G. Barriga, M. N. Holme and M. M. Stevens, *Angew. Chem., Int. Ed.*, 2019, **58**, 2958–2978.
4 B. P. Dyett, H. Yu, J. Strachan, C. J. Drummond and C. E. Conn, *Nat. Commun.*, 2019, **10**, 4492.
5 E. M. Landau and J. P. Rosenbusch, *Proc. Natl. Acad. Sci. U. S. A.*, 1996, **93**, 14532–14535.
6 E. M. Landau, G. Rummel, S. W. Cowan-Jacob and J. P. Rosenbusch, *J. Phys. Chem. B*, 1997, **101**, 1935–1937.
7 A. M. Squires, R. H. Templer, J. M. Seddon, J. Woenckhaus, R. Winter, S. Finet and N. Theyencheri, *Langmuir*, 2002, **18**, 7384–7392.
8 G. C. Shearman, O. Ces, R. H. Templer and J. M. Seddon, *J. Phys.: Condens. Matter*, 2006, **18**, S1105–S1124.
9 G. C. Shearman, B. J. Khoo, M.-L. Motherwell, K. A. Brakke, O. Ces, C. E. Conn, J. M. Seddon and R. H. Templer, *Langmuir*, 2007, **23**, 7276–7285.
10 C. E. Conn, O. Ces, A. M. Squires, X. Mulet, R. Winter, S. M. Finet, R. H. Templer and J. M. Seddon, *Langmuir*, 2008, **24**, 2331–2340.
11 G. C. Shearman, O. Ces and R. H. Templer, *Soft Matter*, 2010, **6**, 256–262.
12 A. I. I. Tyler, H. M. G. Barriga, E. S. Parsons, N. L. C. McCarthy, O. Ces, R. V. Law, J. M. Seddon and N. J. Brooks, *Soft Matter*, 2015, **11**, 3279–3286.
13 H. M. G. Barriga, A. I. I. Tyler, N. L. C. McCarthy, E. S. Parsons, O. Ces, R. V. Law, J. M. Seddon and N. J. Brooks, *Soft Matter*, 2015, **11**, 600–607.
14 L. Van't Hag, S. L. Gras, C. E. Conn and C. J. Drummond, *Chem. Soc. Rev.*, 2017, **46**, 2705–2731.
15 M. Caffrey, *Acta Crystallogr., Sect. F: Struct. Biol. Commun.*, 2015, **71**, 3–18.
16 S. Hyde, B. W. Ninham, S. Andersson, K. Larsson, T. Landh, Z. Blum and S. Lidin, *The Language of Shape*, Elsevier, 1997.
17 C. V. Kulkarni, W. Wachter, G. Iglesias-Salto, S. Engelskirchen and S. Ahualli, *Phys. Chem. Chem. Phys.*, 2011, **13**, 3004–3021.
18 G. Porte, J. Appell, P. Bassereau and J. Marignan, *J. Phys.*, 1989, **50**, 1335–1347.
19 L. Porcar, W. A. Hamilton, P. D. Butler and G. G. Warr, *Phys. Rev. Lett.*, 2004, **93**, 198301.
20 A. Bhattacharya, H. Niederholtmeyer, K. A. Podolsky, R. Bhattacharya, J.-J. Song, R. J. Brea, C.-H. Tsai, S. K. Sinha and N. K. Devaraj, *Proc. Natl. Acad. Sci. U. S. A.*, 2020, **117**, 18206–18215.
21 M. Valldeperas, M. Talaikis, S. K. Dhayal, M. Velicka, J. Barauskas, G. Niaura and T. Nylander, *Biophys. J.*, 2019, **117**, 829–843.
22 A. M. Seddon, G. Lotze, T. S. Plivelic and A. M. Squires, *J. Am. Chem. Soc.*, 2011, **133**, 13860–13863.
23 A. M. Squires, J. E. Hallett, C. M. Beddoes, T. S. Plivelic and A. M. Seddon, *Langmuir*, 2013, **29**, 1726–1731.
24 T. Oka and H. Hojo, *Langmuir*, 2014, **30**, 8253–8257.
25 A. Ridell, *Colloids Surf., A*, 2003, **228**, 17–24.
26 V. Cherezov, J. Clogston, M. Z. Papiz and M. Caffrey, *J. Mol. Biol.*, 2006, **357**, 1605–1618.
27 H. Evenbratt, L. Nordstierna, M. B. Ericson and S. Engström, *Langmuir*, 2013, **29**, 13058–13065.
28 V. Cherezov, D. M. Rosenbaum, M. A. Hanson, S. G. F. Rasmussen, F. S. Thian, T. S. Kobilka, H.-J. Choi, P. Kuhn, W. I. Weis, B. K. Kobilka and R. C. Stevens, *Science*, 2007, **318**, 1258–1265.
29 S. G. F. Rasmussen, B. T. DeVree, Y. Zou, A. C. Kruse, K. Y. Chung, T. S. Kobilka, F. S. Thian, P. S. Chae, E. Pardon, D. Calinski, J. M. Mathiesen, S. T. A. Shah, J. A. Lyons, M. Caffrey, S. H. Gellman, J. Steyaert, G. Skiniotis, W. I. Weis, R. K. Sunahara and B. K. Kobilka, *Nature*, 2011, **477**, 549–555.

30 P. Wadsten-Hindrichsen, J. Bender, J. Unga and S. Engström, *J. Colloid Interface Sci.*, 2007, **315**, 701–713.
31 S. Engström, K. Alfons, M. Rasmusson and H. Ljusberg-Wahren, *Progress in Colloid & Polymer Science*, Steinkopff, 1998, pp. 93–98.
32 M. Caffrey, *Cryst. Growth Des.*, 2008, **8**, 4244–4254.
33 D. Li, N. Howe, A. Dukkipati, S. T. A. Shah, B. D. Bax, C. Edge, A. Bridges, P. Hardwicke, O. M. P. Singh, G. Giblin, A. Pautsch, R. Pfau, G. Schnapp, M. Wang, V. Olieric and M. Caffrey, *Cryst. Growth Des.*, 2014, **14**, 2034–2047.
34 P. Wadsten, A. B. Wöhri, A. Snijder, G. Katona, A. T. Gardiner, R. J. Cogdell, R. Neutze and S. Engström, *J. Mol. Biol.*, 2006, **364**, 44–53.
35 A. B. Wöhri, L. C. Johansson, P. Wadsten-Hindrichsen, W. Y. Wahlgren, G. Fischer, R. Horsefield, G. Katona, M. Nyblom, F. Öberg, G. Young, R. J. Cogdell, N. J. Fraser, S. Engström and R. Neutze, *Structure*, 2008, **16**, 1003–1009.
36 A. B. Wöhri, W. Y. Wahlgren, E. Malmerberg, L. C. Johansson, R. Neutze and G. Katona, *Biochemistry*, 2009, **48**, 9831–9838.
37 A. Zabara, T. G. Meikle, R. Trenker, S. Yao, J. Newman, T. S. Peat, F. Separovic, C. E. Conn, M. J. Call, M. E. Call, E. M. Landau and C. J. Drummond, *Cryst. Growth Des.*, 2017, **17**, 5667–5674.
38 Jason Briggs, Hesson Chung and Martin Caffrey, *J. Phys. II*, 1996, **6**, 723–751.
39 H. Qiu and M. Caffrey, *Biomaterials*, 2000, **21**, 223–234.
40 J. N. Israelachvili, *Intermolecular and Surface Forces*, Elsevier, 2011.
41 V. Cherezov, J. Clogston, Y. Misquitta, W. Abdel-Gawad and M. Caffrey, *Biophys. J.*, 2002, **83**, 3393–3407.
42 R. F. Service, *Science*, 2014, **343**, 1094–1097.
43 C. Brasnett, G. Longstaff, L. Compton and A. Seddon, *Sci. Rep.*, 2017, **7**, 8229.
44 H. Kim, Z. Song and C. Leal, *Proc. Natl. Acad. Sci. U. S. A.*, 2017, **114**, 10834–10839.
45 A. Zabara, J. T. Y. Chong, I. Martiel, L. Stark, B. A. Cromer, C. Speziale, C. J. Drummond and R. Mezzenga, *Nat. Commun.*, 2018, **9**, 544.
46 S. S. W. Leung and C. Leal, *Soft Matter*, 2019, **15**, 1269–1277.
47 B. Angelov, A. Angelova, R. Mutafchieva, S. Lesieur, U. Vainio, V. M. Garamus, G. V. Jensen and J. S. Pedersen, *Phys. Chem. Chem. Phys.*, 2011, **13**, 3073–3081.
48 M. Talaikis, M. Valldeperas, I. Matulaitiene, J. L. Borzova, J. Barauskas, G. Niaura and T. Nylander, *J. Phys. Chem. B*, 2019, **123**, 2662–2672.
49 S. Chakraborty, M. Doktorova, T. R. Molugu, F. A. Heberle, H. L. Scott, B. Dzikovski, M. Nagao, L.-R. Stingaciu, R. F. Standaert, F. N. Barrera, J. Katsaras, G. Khelashvili, M. F. Brown and R. Ashkar, *Proc. Natl. Acad. Sci. U. S. A.*, 2020, **117**, 21896–21905.
50 R. S. Gracià, N. Bezlyepkina, R. L. Knorr, R. Lipowsky and R. Dimova, *Soft Matter*, 2010, **6**, 1472.
51 D. L. Gater, V. Réat, G. Czaplicki, O. Saurel, A. Milon, F. Jolibois and V. Cherezov, *Langmuir*, 2013, **29**, 8031–8038.
52 F. de Meyer and B. Smit, *Proc. Natl. Acad. Sci. U. S. A.*, 2009, **106**, 3654–3658.
53 A. A. Polyansky, P. E. Volynsky, D. E. Nolde, A. S. Arseniev and R. G. Efremov, *J. Phys. Chem. B*, 2005, **109**, 15052–15059.
54 M. Pasenkiewicz-Gierula, Y. Takaoka, H. Miyagawa, K. Kitamura and A. Kusumi, *J. Phys. Chem. A*, 1997, **101**, 3677–3691.
55 S. Leekumjorn and A. K. Sum, *Biophys. J.*, 2006, **90**, 3951–3965.
56 A. H. de Vries, A. E. Mark and S. J. Marrink, *J. Phys. Chem. B*, 2004, **108**, 2454–2463.
57 W. Hübner and A. Blume, *Chem. Phys. Lipids*, 1998, **96**, 99–123.
58 X. Ai and M. Caffrey, *Biophys. J.*, 2000, **79**, 394–405.
59 Y. Misquitta and M. Caffrey, *Biophys. J.*, 2003, **85**, 3084–3096.
60 C. Sennoga, A. Heron, J. M. Seddon, R. H. Templer and B. Hankamer, *Acta Crystallogr., Sect. D: Biol. Crystallogr.*, 2003, **59**, 239–246.
61 B. R. Pauw, A. J. Smith, T. Snow, O. Shebanova, J. P. Sutter, J. Ilavsky, D. Hermida-Merino, G. J. Smales, N. J. Terrill, A. F. Thünemann and W. Bras, *J. Synchrotron Radiat.*, 2021, **28**, 824–833.
62 L. C. Johansson, D. Arnlund, T. A. White, G. Katona, D. P. DePonte, U. Weierstall, R. B. Doak, R. L. Shoeman, L. Lomb, E. Malmerberg, J. Davidsson, K. Nass, M. Liang, J. Andreasson, A. Aquila, S. Bajt, M. Barthelmess, A. Barty, M. J. Bogan, C. Bostedt, J. D. Bozek, C. Caleman, R. Coffee, N. Coppola, T. Ekeberg, S. W. Epp, B. Erk, H. Fleckenstein, L. Foucar, H. Graafsma, L. Gumprecht, J. Hajdu, C. Y. Hampton, R. Hartmann, A. Hartmann, G. Hauser, H. Hirsemann, P. Holl, M. S. Hunter, S. Kassemeyer, N. Kimmel, R. A. Kirian, F. R. N. C. Maia, S. Marchesini, A. V. Martin, C. Reich, D. Rolles, B. Rudek, A. Rudenko, I. Schlichting, J. Schulz, M. M. Seibert, R. G. Sierra, H. Soltau, D. Starodub, F. Stellato, S. Stern, L. Strüder, N. Timneanu, J. Ullrich, W. Y. Wahlgren, X. Wang, G. Weidenspointner, C. Wunderer, P. Fromme, H. N. Chapman, J. C. H. Spence and R. Neutze, *Nat. Methods*, 2012, **9**, 263–265.
63 A. M. Seddon, *Advances in Planar Lipid Bilayers and Liposomes*, Elsevier, 2013, pp. 147–180.
64 R. Neutze, G. Brändén and G. F. Schertler, *Curr. Opin. Struct. Biol.*, 2015, **33**, 115–125.
65 G. Selikhanov, T. Fufina, L. Vasilieva, C. Betzel and A. Gabdulkhakov, *IUCrJ*, 2020, **7**, 1084–1091.